Supporting Information

Two-Dimensional Trilayer Heterostructures with Cascade Dual Z-Schemes to Achieve Efficient Hydrogen Evolution Reaction

Xue-Qing Wan [a], Chuan-Lu Yang [a,b,*], Xiao-Hu Li[b,c], Yu-Liang Liu [a], and Wen-Kai Zhao [a]

[a] *School of Physics and Optoelectronic Engineering, Ludong University, Yantai 264025, China*
[b] *Xinjiang Astronomical Observatory, Chinese Academy of Sciences, Urumqi 830011, China*
[c] *Key Laboratory of Radio Astronomy, Chinese Academy of Sciences, Urumqi 830011, China*

1. The geometrical configurations and electronic properties of the monolayers and heterostructures

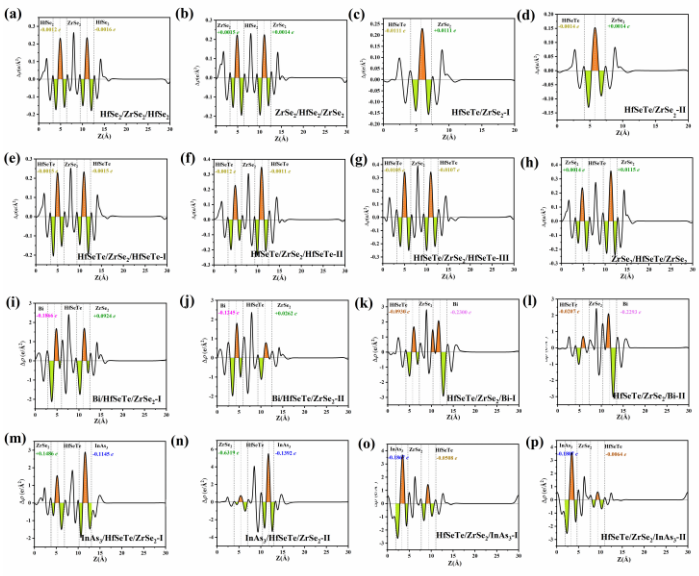

Fig. S1. The plane-integrated charge density differences along with *z*-direction for 16 heterostructures. The orange and green regions represent electron accumulation and depletion, respectively. (a) $HfSe_2/ZrSe_2/HfSe_2$, (b) $ZrSe_2/HfSe_2/ZrSe_2$, (c) HfSeTe/$ZrSe_2$-I, (d) HfSeTe/$ZrSe_2$-II, (e) HfSeTe/$ZrSe_2$/HfSeTe-I, (f) HfSeTe/$ZrSe_2$/HfSeTe-II, (g) HfSeTe/$ZrSe_2$/HfSeTe-III, (h) $ZrSe_2$/HfSeTe/$ZrSe_2$, (i) Bi/HfSeTe/$ZrSe_2$-I, (j) Bi/HfSeTe/$ZrSe_2$-II, (k) HfSeTe/$ZrSe_2$/Bi-I, (l) HfSeTe/$ZrSe_2$/Bi-II, (m) $InAs_3$/HfSeTe/$ZrSe_2$-I, (n) $InAs_3$/HfSeTe/$ZrSe_2$-II, (o) HfSeTe/$ZrSe_2$/$InAs_3$-I, and (p) HfSeTe/$ZrSe_2$/$InAs_3$-II.

*Corresponding author. *E-mail address:* ycl@ldu.edu.cn. (C.L. Yang).

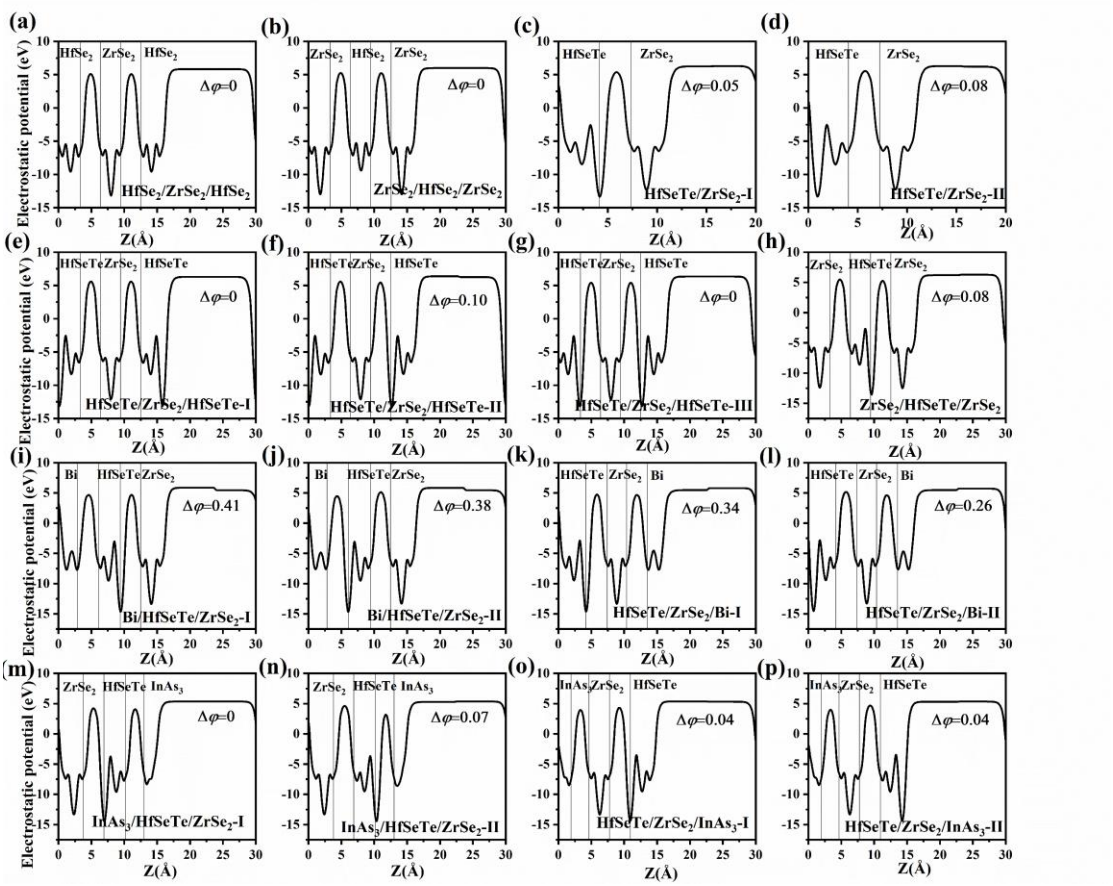

Fig. S2. The electrostatic potentials of the considered heterostructures. (a) $HfSe_2/ZrSe_2/HfSe_2$, (b) $ZrSe_2/HfSe_2/ZrSe_2$, (c) HfSeTe/$ZrSe_2$-I, (d) HfSeTe/$ZrSe_2$-II, (e) HfSeTe/$ZrSe_2$/HfSeTe-I, (f) HfSeTe/$ZrSe_2$/HfSeTe-II, (g) HfSeTe/$ZrSe_2$/HfSeTe-III, (h) $ZrSe_2$/HfSeTe/$ZrSe_2$, (i) Bi/HfSeTe/$ZrSe_2$-I, (j) Bi/HfSeTe/$ZrSe_2$-II, (k) HfSeTe/$ZrSe_2$/Bi-I, (l) HfSeTe/$ZrSe_2$/Bi-II, (m) $InAs_3$/HfSeTe/$ZrSe_2$-I, (n) $InAs_3$/HfSeTe/$ZrSe_2$-II, (o) HfSeTe/$ZrSe_2$/$InAs_3$-I, and (p) HfSeTe/$ZrSe_2$/$InAs_3$-II.

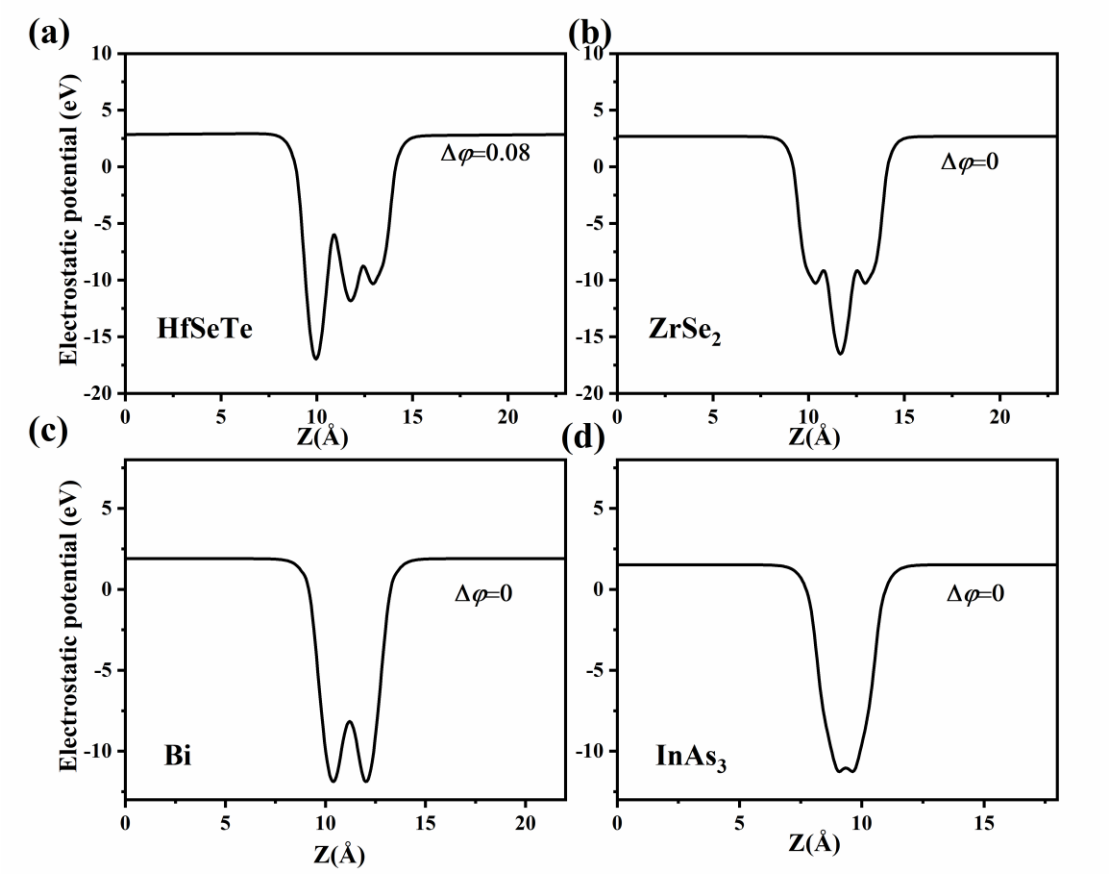

Fig. S3. The electrostatic potentials of the monolayers. (a) HfSeTe, (b) $ZrSe_2$, (c) Bi, (d) $InAs_3$.

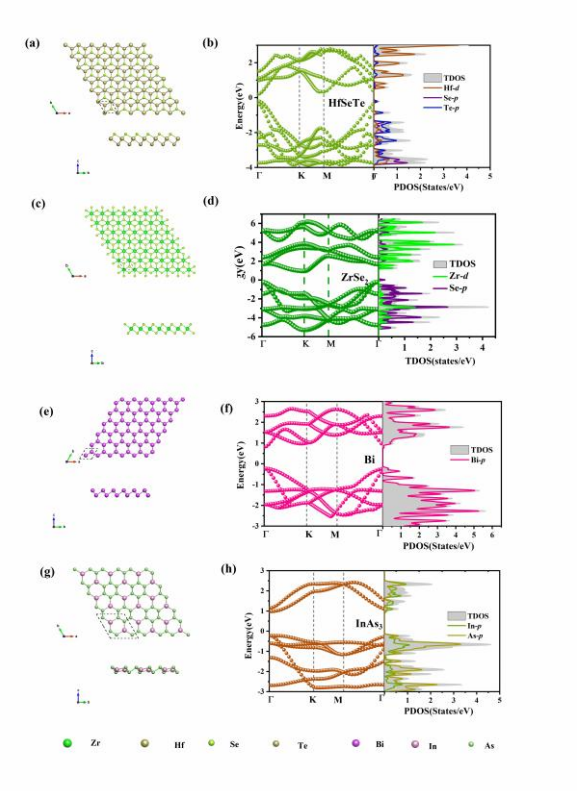

Fig. S4. The geometrical structures, band structures, and project density of states. (a), (b) HfSeTe, (c), (d) $ZrSe_2$, (e), (f) Bi, and (g), (h) $InAs_3$ monolayers. The Fermi level is set to zero.

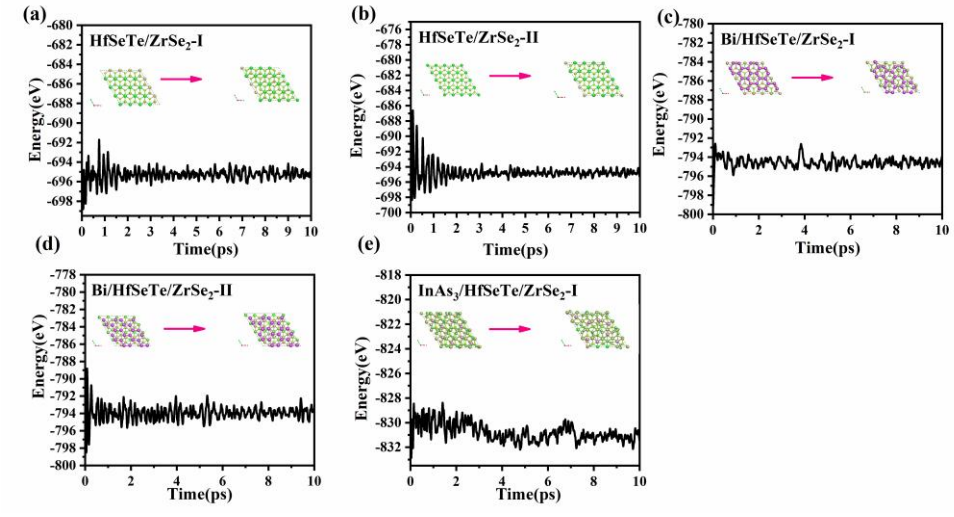

Fig. S5. The AIMD simulation results in a temperature of 300 K for the considered structures. (a) HfSeTe/$ZrSe_2$-I, (b) HfSeTe/$ZrSe_2$-II, (c) Bi/HfSeTe/$ZrSe_2$-I, (d) Bi/HfSeTe/$ZrSe_2$-II, and (e) $InAs_3$/HfSeTe/$ZrSe_2$-I.

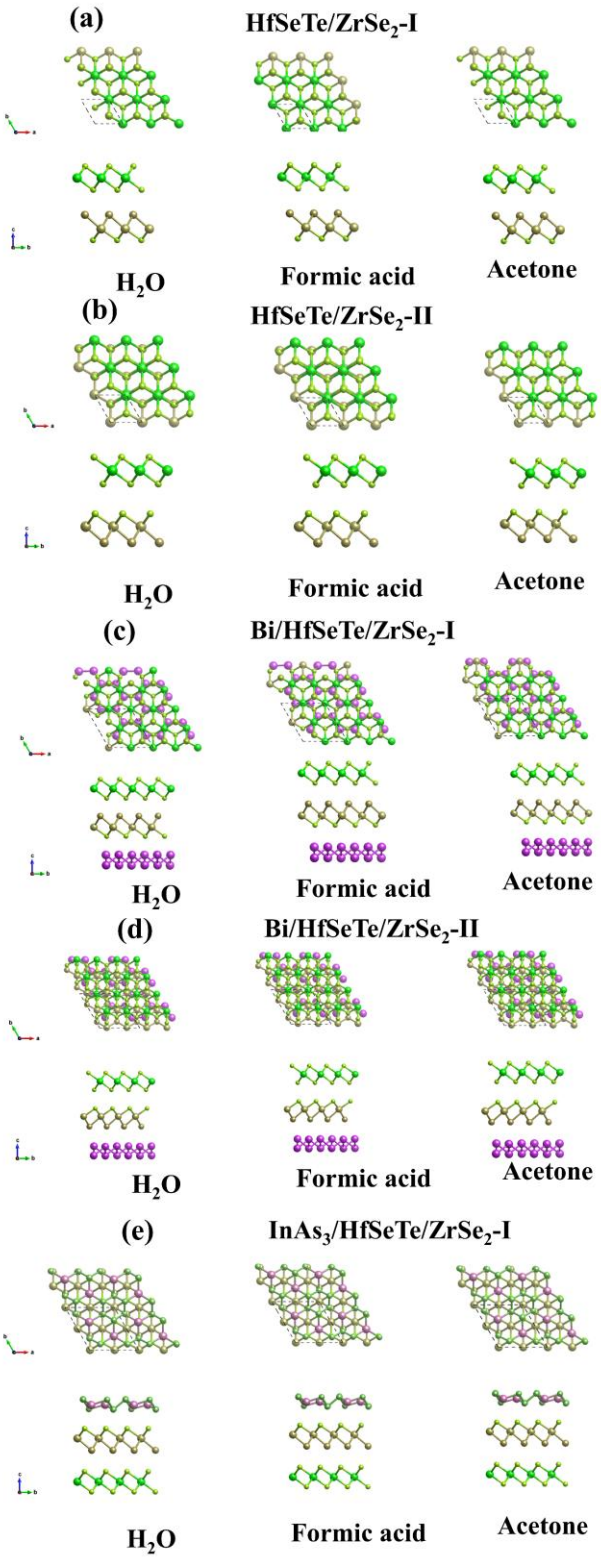

Fig. S6. The geometric structures of (a) $HfSeTe/ZrSe_2$-I, (b) $HfSeTe/ZrSe_2$-II, (c) $Bi/HfSeTe/ZrSe_2$-I, (d) $Bi/HfSeTe/ZrSe_2$-II, and (e) $InAs_3/HfSeTe/ZrSe_2$-I optimized by VASPsol in the water, formic acid, and acetone, respectively.

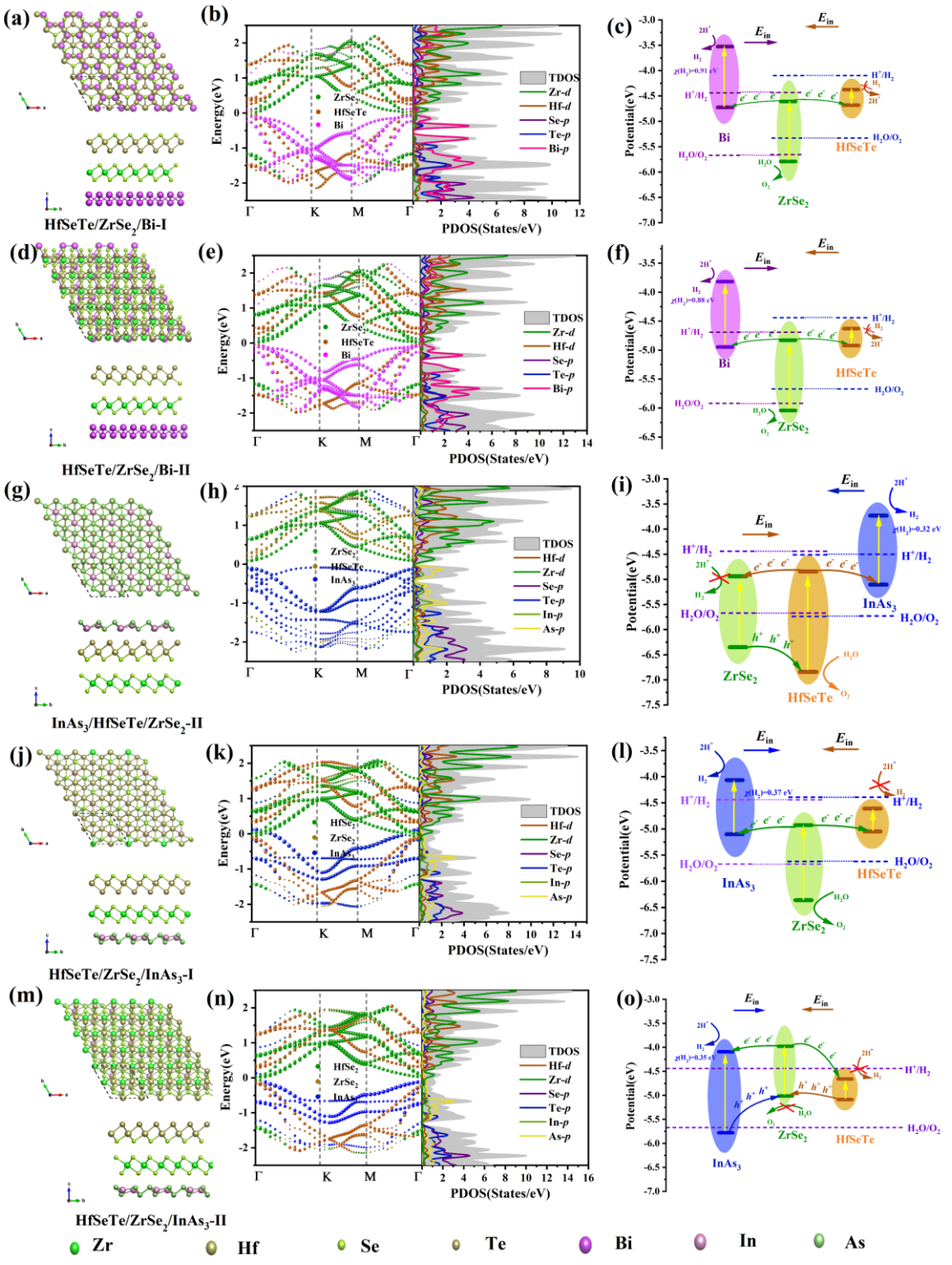

Fig. S7. The geometric structures, band structures, project density of states, and photocatalytic schemes. (a)-(c) $HfSeTe/ZrSe_2$/Bi-I, (d)-(f) $HfSeTe/ZrSe_2$/Bi-II, (g)-(i) $InAs_3/HfSeTe/ZrSe_2$-II, (j)-(l) $HfSeTe/ZrSe_2/InAs_3$-I, and (m)-(o) $HfSeTe/ZrSe_2/InAs_3$-II.

Table S1. The interlayer distances (d_1, d_2), formation energies (E_f), reduction potentials (P_r), oxidation potentials (P_o), and η'_{STH}s of the 16 configurations for heterostructure optimized and calculated by HSE06. The interlayer distances between the bottom layer and middle layer are represented by d_1 and the interlayer distances between the bottom layer and middle layer are presented by d_2.

Configuration	d_1 (Å)	d_2 (Å)	E_f (meV/ Å^2)	P_r (eV)	P_o (eV)	η'_{STH} (%)
$HfSe_2/ZrSe_2/HfSe_2$	3.80	3.78	35.74	-4.74/-4.74	-6.29	-
$ZrSe_2/HfSe_2/ZrSe_2$	3.79	3.78	37.82	-4.72	-6.35/-6.37	-
HfSeTe/$ZrSe_2$-I	3.87	-	21.65	-4.41	-6.49	22.08
HfSeTe/$ZrSe_2$-II	3.85	-	19.48	-4.44	-6.52	-
HfSeTe/$ZrSe_2$/HfSeTe-I	3.79	3.81	37.82	-4.46/-4.39	-6.38	-
HfSeTe/$ZrSe_2$/HfSeTe-II	3.84	3.85	40.44	-4.36/-4.51	-6.20/-6.31	-
HfSeTe/$ZrSe_2$/HfSeTe-III	3.88	3.85	42.57	-4.41/-4.52	-6.16	-
$ZrSe_2$/HfSeTe/$ZrSe_2$	3.77	3.82	39.93	-4.54/-4.46	-6.16	-
Bi/HfSeTe/$ZrSe_2$-I	3.75	3.47	38.24	-3.62	-6.19	40.52
Bi/HfSeTe/$ZrSe_2$-II	3.73	3.74	34.94	-3.56	-6.18	39.47
HfSeTe/$ZrSe_2$/Bi-I	3.45	3.77	39.04	-3.53/-4.72	-6.13/-5.79	-
HfSeTe/$ZrSe_2$/Bi-II	3.32	3.75	33.89	-3.56/-4.63	-6.04/-5.79	-
$InAs_3$/HfSeTe/$ZrSe_2$-I	3.78	3.52	39.82	-4.12	-6.38	41.04
$InAs_3$/HfSeTe/$ZrSe_2$-II	3.83	3.54	44.46	-4.93/-3.66	-6.94/-6.77	-
HfSeTe/$ZrSe_2$/$InAs_3$-I	3.46	3.80	41.64	-4.07/-4.66	-6.36/-6.41	-
HfSeTe/$ZrSe_2$/$InAs_3$-II	3.37	3.72	37.61	-4.09/-4.66	-5.03	-

Table S2. The lattice constants (a), bandgaps (E_g), CBMs, and VBMs were calculated by HSE06 for HfSeTe, $ZrSe_2$, Bi, and $InAs_3$ monolayers.

Monolayer	a (Å)	a (Å) (Exp./Cal.)	E_g(eV)	E_g(eV) (Exp./Cal.)	CBM (eV)	VBM (eV)
HfSeTe	3.92	3.85[1],3.82[2]	0.39	0.47[1],0.44[2]	-4.62	-5.05
$ZrSe_2$	3.76	3.77[3,4]	1.15	1.20[5],1.18[6]	-4.99	-6.15
Bi	4.22	4.24[7]	1.02	1.16[7]	-3.27	-4.31
$InAs_3$	7.85	-	1.19	-	-3.97	-5.15

Table S3. The solvation energy (ΔE_{sol}) of the structures we considered in the water, formic acid, and acetone solutions calculated by VASPsol.

	ΔE_{sol}-water (eV)	ΔE_{sol}-formic acid(eV)	ΔE_{sol}-acetone(eV)
HfSeTe/$ZrSe_2$-I	-0.0232	-0.0217	-0.0199
HfSeTe/$ZrSe_2$-II	-0.0083	-0.0076	-0.0052
Bi/HfSeTe/$ZrSe_2$-I	-0.2955	-0.2176	-0.2521
Bi/HfSeTe/$ZrSe_2$-II	-0.3120	-0.2255	-0.2721
$InAs_3$/HfSeTe/$ZrSe_2$-I	-0.3941	-0.3923	-0.3301

2. Details of calculations for the optical properties and the Solar-to-hydrogen (η'_{STH})

The Eq. of optical absorption coefficient $\alpha(\omega)$ is [8,9]

$$\alpha(\omega) = \sqrt{2}\sqrt{\sqrt{\varepsilon_r^2(\omega) + \varepsilon_i^2}(\omega) - \varepsilon_r(\omega)} \quad (2)$$

Where $\varepsilon_i(\omega)$ is the imaginary part of the complex dielectric function $\varepsilon(\omega) = \varepsilon_r(\omega) + i\varepsilon_i(w)$, can be calculated by following Equation [10]:

$$\varepsilon_i(\omega) = \frac{4\pi^2}{m^2\omega^2}\Sigma_{c,v}\int_{Bz}\frac{2}{(2\pi)^3}\left|M_{c,v}(k)\right|^2\delta(\varepsilon_{ck} - \varepsilon_{vk} - h_\omega)d^3k \quad (3)$$

Where $\left|M_{c,v}(k)\right|^2$ represent the momentum matrix element, c, and v represent the conduction and valence band states, respectively. $\varepsilon_i(\omega)$ can be calculated by VASP.

The real part $\varepsilon_r(\omega)$ can be calculated from the imaginary part $\varepsilon_i(\omega)$ of the complex dielectric function by using the Kramer-Kroning relationship [11].

The solar-to-hydrogen efficiency (η_{STH}) is the result of the efficiency of light absorption η_{abs} and the efficiency of carrier utilization η_{cu}, which can be considered as the crucial factor in determining the catalytic ability of photocatalysts. We calculated $\eta_{\mathrm{STH}}, \eta_{\mathrm{abs}}$, and η_{cu} based on the following formula [12]:

$$\eta_{\mathrm{STH}} = \eta_{\mathrm{abs}} \times \eta_{\mathrm{cu}} \tag{4}$$

$$\eta_{\mathrm{abs}} = \frac{\int_{E_{\mathrm{g}}}^{\infty} P(\hbar\omega)\, d(\hbar\omega)}{\int_{0}^{\infty} P(\hbar\omega)\, d(\hbar\omega)} \tag{5}$$

$$\eta_{\mathrm{cu}} = \frac{\Delta G \int_{E}^{\infty} \frac{P(\hbar\omega)}{\hbar\omega} d(\hbar\omega)}{\int_{E_{\mathrm{g}}}^{\infty} P(\hbar\omega)\, d(\hbar\omega)} \tag{6}$$

$$E = \begin{cases} E_{\mathrm{g}}, \ (\chi(\mathrm{H_2}) \geq 0.2, \chi(\mathrm{O_2}) \geq 0.6) \\ E_{\mathrm{g}} + 0.2 - \chi(\mathrm{H_2}), (\chi(\mathrm{H_2}) < 0.2, \chi(\mathrm{O_2}) \geq 0.6) \\ E_{\mathrm{g}} + 0.6 - \chi(\mathrm{O_2}), (\chi(\mathrm{H_2}) \geq 0.2, \chi(\mathrm{O_2}) < 0.6) \\ E_{\mathrm{g}} + 0.8 - \chi(\mathrm{H_2}) - \chi(\mathrm{O_2}), (\chi(\mathrm{H_2}) < 0.2, \chi(\mathrm{O_2}) < 0.6) \end{cases} \tag{7}$$

Where $P\,(\hbar\omega)$ is the AM1.5G solar energy flux at the photo energy $\hbar\omega$; E_g (HSE) is the bandgap of the layer materials; $\chi(\mathrm{H_2})$ and $\chi(\mathrm{O_2})$ are the overpotentials for hydrogen and oxygen evolution reactions, respectively. ΔG represents the potential difference of 1.23 eV for water splitting, and E is the energy of photons that can actually be utilized for water splitting.

Because the intrinsic electric field would promote the electron-hole separation, the corrected STH efficiency (η'_{STH}) for polarized materials in photocatalytic water splitting reaction can be calculated as:

$$\eta'_{\mathrm{STH}} = \eta_{\mathrm{STH}} \times \frac{\int_{0}^{\infty} P(\hbar\omega)\mathrm{d}(\hbar\omega)}{\int_{0}^{\infty} P(\hbar\omega)\mathrm{d}(\hbar\omega) + \Delta\Phi \int_{0}^{\infty} P(\hbar\omega)\mathrm{d}(\hbar\omega)} \tag{8}$$

Where $\Delta\Phi$ is the vacuum level difference between the two respective surfaces of the polarized material.

Table S4. The energy conversion efficiency of the light absorption of light (η_{abs}), carrier utilization (η_{cu}), and η'_{STH} of the Bi/HfSeTe/$ZrSe_2$-I heterostructure.

Bi/HfSeTe/$ZrSe_2$	$E_{g\text{-}Bi}$ (eV)	$E_{g\text{-}HfSeTe}$ (eV)	$E_{g\text{-}ZrSe2}$ (eV)	$\chi(H_2)$ (eV)	$\chi(O_2)$ (eV)	$\Delta\varphi$ (eV)	η_{abs} (%)	η_{cu} (%)	η'_{STH} (%)
-2%	1.12	0.33	0.99	0.94	0.37	0.55	82.74	52.03	34.60
-1%	1.03	0.35	1.07	0.86	0.40	0.47	84.98	54.78	38.21
0%	1.04	0.37	1.17	0.81	0.52	0.41	80.94	58.86	40.52
1%	1.05	0.44	1.26	0.76	0.62	0.35	75.38	62.48	41.53
2%	1.04	0.51	1.35	0.71	0.70	0.31	71.97	60.96	39.00
3%	1.03	0.58	1.42	0.76	0.68	0.31	68.19	59.43	36.77
4%	0.97	0.67	1.55	0.89	0.65	0.32	60.70	56.52	31.50

Table S5. The energy conversion efficiency of the light absorption of light (η_{abs}), carrier utilization (η_{cu}), and η'_{STH} of the Bi/HfSeTe/$ZrSe_2$-II heterostructure.

Bi/HfSeTe/$ZrSe_2$	$E_{g\text{-}Bi}$ (eV)	$E_{g\text{-}HfSeTe}$ (eV)	$E_{g\text{-}ZrSe2}$ (eV)	$\chi(H_2)$ (eV)	$\chi(O_2)$ (eV)	$\Delta\varphi$ (eV)	η_{abs} (%)	η_{cu} (%)	η'_{STH} (%)
-3%	1.13	0.27	0.88	1.05	0.24	0.54	83.34	44.40	29.77
-2%	1.13	0.28	0.98	0.98	0.33	0.48	83.34	49.36	34.18
-1%	1.12	0.32	1.08	0.91	0.43	0.42	83.85	54.47	38.36
0%	1.13	0.38	1.20	0.88	0.51	0.38	79.11	57.73	39.47
1%	1.09	0.47	1.26	0.83	0.60	0.38	75.38	62.48	41.12
2%	1.03	0.56	1.35	0.80	0.68	0.39	71.97	60.96	38.63
3%	0.98	0.66	1.43	0.76	0.76	0.40	67.59	59.19	35.40
4%	0.94	0.75	1.49	0.71	0.82	0.40	64.03	57.79	33.03

Table S6. The energy conversion efficiency of the light absorption of light (η_{abs}), carrier utilization (η_{cu}), and η'_{STH} of the $InAs_3$/HfSeTe/$ZrSe_2$-I heterostructure.

$InAs_3$/HfSeTe/$ZrSe_2$	$E_{\text{g-InAs3}}$ (eV)	$E_{\text{g-HfSeTe}}$ (eV)	$E_{\text{g-ZrSe2}}$ (eV)	$\chi(H_2)$ (eV)	$\chi(O_2)$ (eV)	$\Delta\varphi$ (eV)	η_{abs} (%)	η_{cu} (%)	η'_{STH} (%)
-3%	0.64	0.24	1.16	0.24	0.46	0.24	81.54	55.64	41.09
-2%	0.70	0.29	1.22	0.28	0.55	0.17	77.86	59.79	43.57
-1%	0.79	0.38	1.33	0.30	0.63	0.10	72.91	61.36	43.16
0%	0.87	0.48	1.41	0.32	0.71	0.00	68.79	59.66	41.04
1%	1.31	0.57	1.49	0.71	0.77	0.03	64.03	57.79	36.67
2%	1.36	0.74	1.65	0.70	0.70	0.08	55.45	54.58	29.68
3%	1.47	0.75	1.62	0.69	0.69	0.14	56.74	55.05	30.16
4%	1.41	0.85	1.68	0.66	0.97	0.17	53.80	53.39	27.93

3. Calculational detail of the NAMD simulation

The nonadiabatic molecular dynamics (NAMD) simulation for the carrier transfer and the electron-hole recombination were carried out by Hefei-NAMD code [13]. The average nonadiabatic coupling (NAC) matrix elements are defined as

$$\mathbf{d}_{ij} = \left\langle \varphi_i \left| \frac{\partial}{\partial t} \right| \varphi_j \right\rangle = \frac{\left\langle \varphi_i | \nabla_R \hat{H} | \varphi_j \right\rangle}{\varepsilon_j - \varepsilon_i} \left(\frac{\partial \mathbf{R}}{\partial t} \right) \quad (9)$$

Where $\mathbf{d}_{ij}$ is the NAC between states *i* and *j*, $\hat{H}$ is the electronic Hamiltonian, φ_{ij}, ε_{ij}, are the wave functions and energies of electronic states *i*/*j*, and $\frac{\partial \mathbf{R}}{\partial t}$ is the velocity of the nuclear.

The decoherence time was computed as the pure-dephasing time in the optical response formalism [14]. The fluctuations are characterized by the energy gap

autocorrelation function (ACF) which defined by [15]

$$C_{(t)} = \frac{\langle \delta U(t)\delta U(t_0)\rangle_T}{\left\langle \left(\delta U(t_0)\right)^2 \right\rangle_T} = \frac{C_{un}(t)}{\langle \Delta E^2(0)\rangle_T} \quad (10)$$

δU is the deviation of the energy gap from the average value, $C_{un}(t)$ is the unnormalized ACF, $C_{(t)}$ is the normalized ACF.

$$\delta U(t) = \Delta E_{ij}\big(\mathbf{R}(t)\big) - \left\langle \Delta E_{ij}\big(\mathbf{R}(t)\big)\right\rangle_T \quad (11)$$

The ΔE_{ij} is the energy difference between *i* and *j* states.

$$D(t) = exp\left[-\frac{\langle (\delta U)^2\rangle_T}{\hbar^2}\int_0^t d\tau_2 \int_0^{\tau_2} d\tau_1\, C(\tau_1)\right] \quad (12)$$

The pure-dephasing time obtained by fitting Supplementary Eq. S18 with Gaussian function.

The spectral density was calculated by applying the Fourier transform of an ACF function [16],

$$I(\omega) = \left|\frac{1}{\sqrt{2\pi}}\int_{-\infty}^{+\infty} dt\, e^{-i\omega t} C(t)\right|^2 \quad (13)$$

The NAMD simulations in this paper were performed in the wavefunction calculated by Perdew-Burke-Ernzerhof (PBE) [17] functional and the eigenenergy with a scissor's operator correction of the bandgap to match those by HSE06 [18-20]. Each state only exhibited slight hybridization with adjacent states in the evolution of 2000 fs, and its values did not change significantly. However, only one electron or one hole was performed to the carrier evolution of CBM or VBM in the simulation. Therefore, we analyzed the evolution of carriers on the six CBMs and VBMs in the heterostructures, and could not divide the nine carrier transfer processes to calculate respectively.

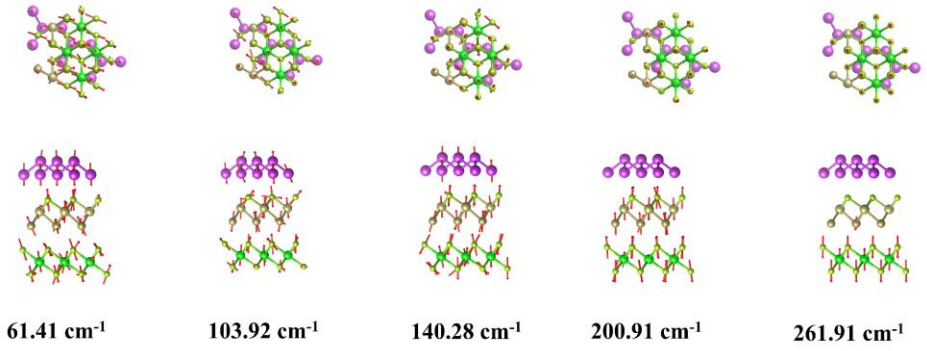

Fig. S8. The lattice vibration modes of the Bi/HfSeTe/$ZrSe_2$-I by VASP.

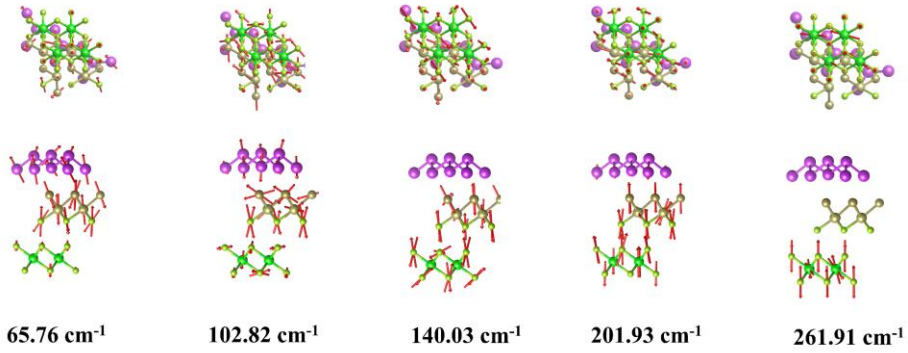

Fig. S9. The lattice vibration modes of the Bi/HfSeTe/$ZrSe_2$-II by VASP.

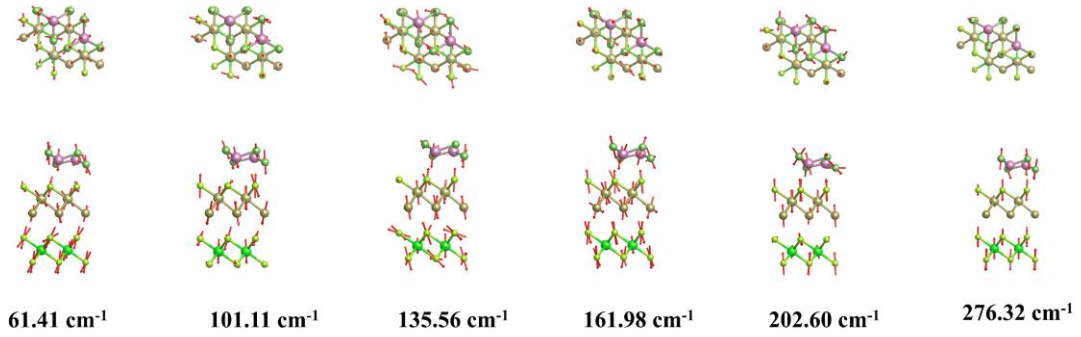

Fig. S10. The lattice vibration modes of the $InAs_3$/HfSeTe/$ZrSe_2$-I by VASP.

Table S7. The NAC elements between the CBMs/VBMs and the other energy states we considered in Bi/HfSeTe/$ZrSe_2$-I.

NAC (eV)	VBM@ $ZrSe_2$	VBM@HfSeTe	VBM@Bi	CBM@$Zr Se_2$	CBM@HfSeTe	CBM@Bi
VBM@$ZrSe_2$	0	8.6E-4	8.6E-4	0.0027	1.3E-4	2.4E-4
VBM-2	0.00138	0.00181	9.8E-4	4.9E-4	3.4E-4	7E-5
VBM-1	0.00112	0.00279	7.3E-4	8.1E-4	3.3E-4	6E-5
VBM@HfSeTe	8.6E-4	0	8E-4	5.1E-4	5.7E-4	6E-5
VBM@Bi	8.6E-4	8E-4	0	0.00189	5.1E-4	7E-5
CBM@$Zr Se_2$	0.0027	5.1E-4	0.00189	0	4.5E-4	1.6E-4
CBM+1	0.00141	4.9E-4	0.0013	0.00979	5.8E-4	1.6E-4

			1			
CBM+2	9.2E-4	4.3E-4	0.0010	0.00362	5.6E-4	1.7E-4
			6			
CBM+3	7.5E-4	3.9E-4	7.5E-4	0.00223	9.7E-4	2.1E-4
CBM@Hf	1.3E-4	5.7E-4	5.1E-4	4.5E-4	0	1.6E-4
SeTe						
CBM+5	1E-4	1.9E-4	1.9E-4	2.5E-4	0.00229	1.4E-4
CBM+6	1.4E-4	3E-4	2.9E-4	3.9E-4	9E-4	2.8E-4
CBM+7	1.6E-4	1.5E-4	1.2E-4	1.4E-4	0.0012	1.9E-4
CBM+8	1.7E-4	8E-5	9E-5	2.4E-4	5.2E-4	3E-4
CBM+9	2.2E-4	8E-5	1.1E-4	2.3E-4	5.2E-4	2.3E-4
CBM+10	1.3E-4	1.3E-4	1.2E-4	1.7E-4	4.4E-4	5.3E-4
CBM+11	1.7E-4	1.5E-4	8E-5	1.7E-4	3.4E-4	8.4E-4
CBM+12	1.4E-4	1.7E-4	9E-5	1.8E-4	3.2E-4	6.7E-4
CBM+13	1.2E-4	1.5E-4	9E-5	1.6E-4	4E-4	7E-4
CBM+14	1.2E-4	1.2E-4	1E-4	1.9E-4	4.1E-4	6.7E-4
CBM+15	2.2E-4	5E-5	9E-5	2.5E-4	1.6E-4	0.002
CBM+16	1.1E-4	6E-5	5E-5	1E-4	1.1E-4	0.0017
						6
CBM+17	2.3E-4	6E-5	6E-5	1.6E-4	1.5E-4	0.0020
						7
CBM@Bi	2.4E-4	6E-5	7E-5	1.6E-4	1.6E-4	0

Table S8. The NAC elements between the CBMs/VBMs and the other energy states we considered in Bi/HfSeTe/$ZrSe_2$-II.

NAC (eV)	VBM@$ZrSe_2$	VBM@HfSeTe	VBM@Bi	CBM@$ZrSe_2$	CBM@HfSeTe	CBM@Bi
VBM@$ZrSe_2$	0	0.00154	6.8E-4	7.2E-4	5.5E-4	4.1E-4
VBM-7	0.02392	0.00128	9E-4	6.9E-4	5.9E-4	5.4E-4
VBM-6	0.00623	0.00133	6.5E-4	6.1E-4	6.3E-4	8.3E-4
VBM-5	0.00277	0.0014	7.7E-4	9.2E-4	4.7E-4	0.00114
VBM-4	0.00324	0.00774	0.00115	9.5E-4	6.7E-4	3.4E-4
VBM@HfSeTe	0.00154	0	0.00264	0.0017	9.1E-4	3.7E-4
VBM-2	9.5E-4	0.01615	0.00498	0.00195	0.00135	3.6E-4
VBM-1	0.00102	0.00399	0.01601	0.00257	0.00185	3.5E-4
VBM@Bi	6.8E-4	0.00264	0	0.00655	0.00223	3.6E-4
CBM@$ZrSe_2$	7.2E-4	0.0017	0.00655	0	0.00189	5.6E-4
CBM+1	6.1E-4	9.9E-4	0.00245	0.01932	0.00253	0.00103
CBM+2	4.6E-4	6.2E-4	0.00181	0.00628	0.00272	0.00142
CBM+3	5.9E-4	5.8E-4	0.00152	0.00277	0.00915	0.00128
CBM@HfSeTe	5.5E-4	9.1E-4	0.00223	0.00189	0	6.9E-4
CBM+5	4.5E-4	0.00116	0.00211	0.00161	0.01575	8.1E-4
CBM+6	5.4E-4	8.4E-4	0.00138	9.8E-4	0.0084	9.5E-4
CBM+7	4.6E-4	6.1E-4	0.00126	0.00104	0.00626	0.00134

CBM+8	4.6E-4	4.9E-4	8E-4	8.7E-4	0.00265	0.00207
CBM+9	4.3E-4	3.5E-4	5.9E-4	9.1E-4	0.00241	0.00271
CBM+10	4.6E-4	7.1E-4	7.1E-4	7.2E-4	0.00226	0.00215
CBM+11	5E-4	4.8E-4	8.2E-4	6.8E-4	0.00166	0.00259
CBM+12	4.8E-4	6.3E-4	7.5E-4	5.9E-4	0.00134	0.00377
CBM+13	4.4E-4	4.9E-4	5.9E-4	6.5E-4	0.00137	0.00482
CBM+14	4.5E-4	4.6E-4	5.1E-4	6.5E-4	0.00124	0.00776
CBM+15	4.7E-4	4.1E-4	4.1E-4	8.1E-4	9E-4	0.01106
CBM+16	4.8E-4	3.6E-4	4.9E-4	6E-4	8.1E-4	0.01861
CBM+17	3.8E-4	3.6E-4	4.2E-4	6E-4	8.3E-4	0.04717
CBM@Bi	4.1E-4	3.7E-4	3.6E-4	5.6E-4	6.9E-4	0

Table S9. The NAC elements between the CBMs/VBMs and the other energy states we considered in $InAs_3$/HfSeTe/$ZrSe_2$-I.

NAC (eV)	VBM@ $ZrSe_2$	VBM@ HfSeTe	VBM@I nAs_3	CBM@Z rSe_2	CBM@Hf SeTe	CBM@ $InAs_3$
VBM@ZrSe 2	0	0.00115	0.00123	0.00128	0.00106	9.5E-4
VBM-8	0.04863	0.00164	0.00131	0.001	0.00107	0.00115
VBM-7	0.01387	0.0022	0.00146	9.1E-4	0.00114	0.00129
VBM-6	0.0073	0.0034	0.00132	0.00108	0.001	0.00173
VBM-5	0.00452	0.00398	0.002	0.00125	0.00125	0.00156
VBM-4	0.00286	0.00528	0.00225	0.00168	0.00143	0.00181
VBM-3	0.00186	0.00851	0.00438	0.00182	0.00162	0.00173
VBM-2	0.00144	0.02308	0.00456	0.00302	0.00196	0.00211

VBM@HfSe Te	0.00115	0	0.01486	0.00377	0.00287	0.00283
VBM@InAs 3	0.00123	0.01486	0	0.01118	0.00267	0.00245
CBM@$ZrSe_2$	0.00128	0.00377	0.01118	0	0.00461	0.00319
CBM+1	0.0014	0.00255	0.00497	0.03472	0.00671	0.0036
CBM+2	0.00132	0.00212	0.00374	0.00999	0.00882	0.00364
CBM+3	0.00129	0.00208	0.00368	0.00748	0.0275	0.00742
CBM@HfSe Te	0.00106	0.00287	0.00267	0.00461	0	0.01721
CBM@Bi	9.5E-4	0.00283	0.00245	0.00319	0.01721	0

4. Calculational method of the Gibbs free energy changes

The ΔG can be calculated by the following Equation [21-23]:

$$\Delta G = \Delta E - T\Delta S + \Delta E_{\mathrm{ZPE}} \quad (14)$$

Where ΔE, ΔE_{ZPE} and ΔS represent the differences in total energy, zero-point energy, and entropy of the slab with and without adsorbed intermediates. T is the temperature 298K. The E_{ZPE} can be calculated by $E_{\mathrm{ZPE}} = \frac{1}{2}\Sigma\hbar\nu$, where the ν is the vibrational frequency over normal modes, and the zero-point of the slab can be negligible. The entropies of the free molecules were taken from the standard tables in Physical chemistry and those of intermediates were obtained from vibrational frequency.

The free energy change for HER electrochemical step can be expressed as:

$\Delta G_{\mathrm{H}*} = G_{\mathrm{H}*} - 1/2 G_{H_2} - G*$ (15)

Then, the free energy change for OER electrochemical steps can be expressed as:

$$\Delta G_1 = G_{OH*} + 1/2G_{H2} - G_{H2O} - G* \quad (16)$$

$$\Delta G_2 = G_{O*} + 1/2G_{H2} - G_{OH*} \quad (17)$$

$$\Delta G_3 = G_{OOH*} + 1/2G_{H2} - G_{H2O} - G_{O*} \quad (18)$$

$$\Delta G_4 = 2G_{H2O} + G* - 3/2G_{H2} - G_{OOH*} + 4.92 \quad (19)$$

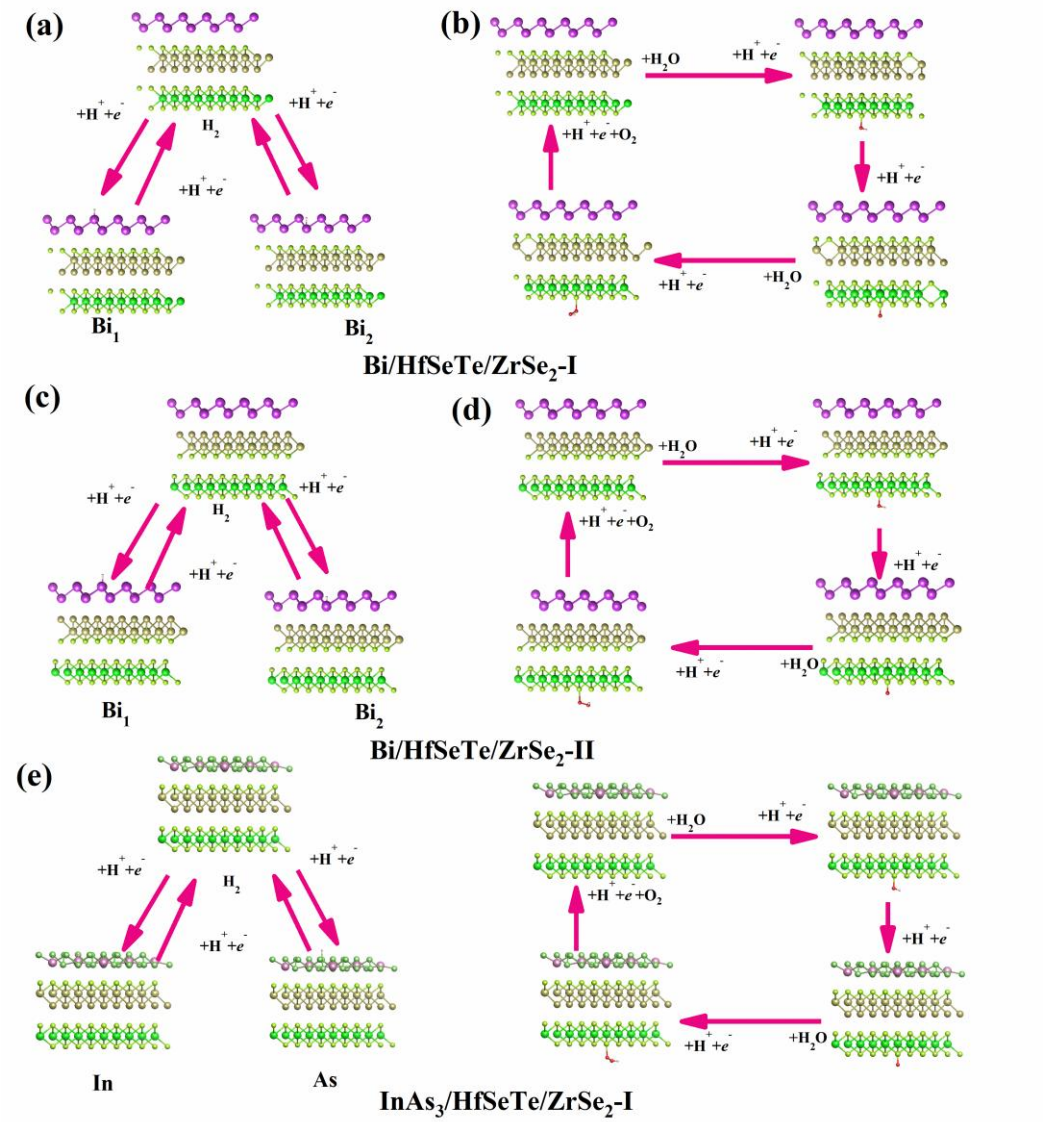

Fig. S11. The adsorption sites for HERs and OERs of the heterostructures. (a), (b) Bi/HfSeTe/$ZrSe_2$-I, (c), (d) Bi/HfSeTe/$ZrSe_2$-II, (e), (f) $InAs_3$/HfSeTe/$ZrSe_2$-I.

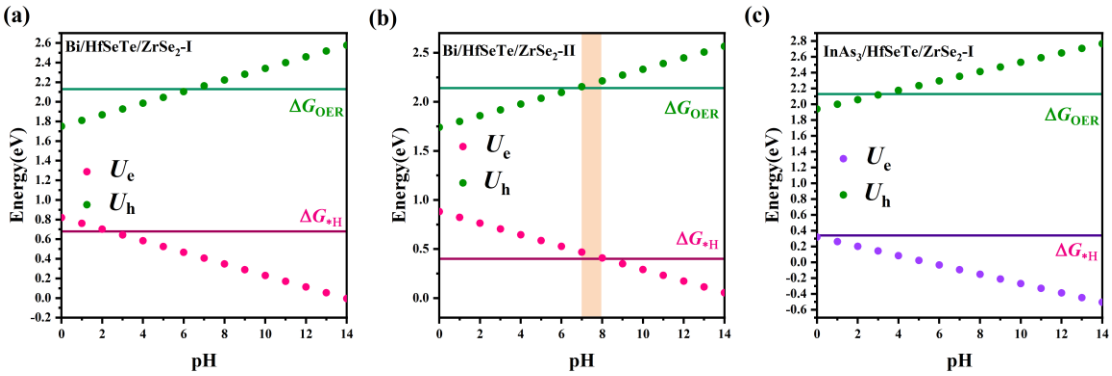

Fig. S12. The value of ΔG_{*H}s and the ΔG_{OER}s changed with the pH. (a) Bi/HfSeTe/$ZrSe_2$-I, (b) Bi/HfSeTe/$ZrSe_2$-II, (c) $InAs_3$/HfSeTe/$ZrSe_2$-I. The orange area represents the pH range of the photocatalytic overall water splitting spontaneously.

Table S10. The absorption energies of H atoms absorbed on different adsorption sites of Bi/HfSeTe/$ZrSe_2$-I, Bi/HfSeTe/$ZrSe_2$-II, and $InAs_3$/HfSeTe/$ZrSe_2$-I. Bi_1 and Bi_2 represent two different adsorption sites of Bi monolayer.

configuration	adsorption sites	absorption energy
Bi/HfSeTe/$ZrSe_2$-I	Bi_1	-2.9188
	Bi_2	-2.8125
Bi/HfSeTe/$ZrSe_2$-II	Bi_1	-3.1699
	Bi_2	-3.1125
$InAs_3$/HfSeTe/$ZrSe_2$-I	In	-3.2537
	As	-3.1462

5. The lattice parameters and coordinates (POSCAR format) for all the structures and the input parameters (INCAR format) for the optimizations of geometrical structures and the static calculations.

Supplemental POSCAR1. The lattice parameters and atom coordinates of Bi/HfSeTe/$ZrSe_2$-I

POSCAR\(1)
1.00000000000000
7.5311473551898782 -0.0000000000000000 0.0000000000000000
-3.7705718095960470 6.5173594027119321 0.0000000000000000
0.0000000000000000 0.0000000000000000 30.0000000000000000
Zr Se Te Hf Bi
4 12 4 4 6
Direct
0.4997011977536749 0.5000889778144652 0.4684285893778699
0.4996971125307432 0.0003130760440218 0.4684514630701644
0.9998709172650061 0.5000518997855065 0.4684806302581451
0.9994943652735063 -0.0001115604286326 0.4683846340308653
0.3332206044936642 0.1667241291072372 0.5205736799078140
0.3330780246877931 0.6665382636860501 0.5206312186995542
0.8331726111225889 0.1666006659815445 0.5206599185464675
0.8330882909705845 0.6669556605591712 0.5205933061917526
0.1663162604286400 0.3338671886828782 0.4161617696445020
0.1663484538543695 0.8333858518156672 0.4161232630603596
0.6661319010493458 0.3332558359976281 0.4161986800993355
0.6664573105868444 0.8334589062791373 0.4161474446616501
0.1646265267282380 0.3314600427244223 0.2015359739116490
0.1680125691967513 0.8362598677287481 0.2016725376549714
0.6683399825651635 0.3362089909128038 0.2005868840037321
0.6652475921327055 0.8325386358462503 0.2017338851181325
0.3291323288327628 0.1676320877774473 0.3137620166777129
0.3381150612071325 0.6719005531829443 0.3133952634632510
0.8335420040261025 0.1677014966951003 0.3134846875688465
0.8326201884759443 0.6612413612248155 0.3136194055786702
0.4987205548957417 0.4985360876460637 0.2517619066086003
0.5008165585879891 -0.0057579189875584 0.2518616701180219
0.9929459311652444 0.5014545401413604 0.2517662406866723
0.0058578349577517 0.0066633085035864 0.2521092872114088
0.3185881866529086 0.9782052797485279 0.0365940557639774
0.6560530608956323 0.6525111612390601 0.0376114534144625
0.9950245643886901 0.3192106510655799 0.0373826032930576
0.3245845193137949 0.3120583267003234 0.0935424246427326
0.6546080289075142 0.9867193171083483 0.0931039990834401

0.9856374080531612 0.6463473504174945 0.0939711866521599

Supplemental POSCAR2. The lattice parameters and atom coordinates of Bi/HfSeTe/$ZrSe_2$-II

```
POSCAR\(2)
  1.00000000000000
    7.5473272924169663   -0.0000000000000000    0.0000000000000000
   -3.7710281195211337    6.5293108208106672    0.0000000000000000
    0.0000000000000000    0.0000000000000000   30.0000000000000000
   Zr   Se   Te   Hf   Bi
    4   12    4    4    6
Direct
  0.4215297251171324  0.4937838314261584  0.4697928884929587
  0.4212654984716432  0.9937206903292500  0.4698139091535737
  0.9215482884278201  0.4937632924734303  0.4698278087247302
  0.9212632842902279  0.9937694936067865  0.4698119040701846
  0.2546721256194144  0.1600399095474161  0.5218589931869234
  0.2546029357702311  0.6600488566655801  0.5218996301543755
  0.7546678734463234  0.1599984109004048  0.5218917304562680
  0.7545382415442596  0.6600879985913101  0.5218877138373753
  0.0877277934845206  0.3268228555522136  0.4177036641090914
  0.0878973266476327  0.8267006296105311  0.4176798180845185
  0.5878316638027804  0.3267464593217904  0.4177259363129499
  0.5879047463411202  0.8267651013022389  0.4177008442504561
  0.8441726233309943  0.3435124521417915  0.3108685556181318
  0.3475345967869988  0.8430662519391463  0.3109140542002063
  0.3478174435473063  0.3449402185928951  0.3109004749537564
  0.8488766157798827  0.8476758562614867  0.3107327960191222
  0.5193098600739599  0.1838145543487534  0.1984284044835257
  0.0154772016076686  0.6784559151523045  0.2002638480071185
  0.0113830349688605  0.1714497089704043  0.1986278900622703
  0.5081188672013248  0.6767154076240800  0.1986384032852498
  0.6809288629798399  0.5048554354163907  0.2606880670973553
  0.1738966678329174  0.0127569121097103  0.2606222601009600
  0.1876104593924285  0.5177481026204799  0.2608267466470182
  0.6794162121124621  0.0109555403228019  0.2610993533249010
  0.2922499528831839  0.9813142544492707  0.0339127975226164
  0.6078341813018699  0.6419280864673766  0.0298861541070025
  0.9544277069543485  0.2988354502248752  0.0326264271419359
  0.2918514412895413  0.3144914501418666  0.0898687991111531
  0.6209605246546701  0.9708918233497870  0.0896117131148243
  0.9417542933386261  0.6363550855394587  0.0842284783694516
```

Supplemental POSCAR3. The lattice parameters and atom coordinates of $InAs_3$/HfSeTe/$ZrSe_2$-II

POSCAR\3
1.00000000000000
7.6692818887248517 -0.0000000000000000 0.0000000000000000
-3.8398322819615616 6.6418966122072254 0.0000000000000000
0.0000000000000000 0.0000000000000000 30.0000000000000000
Hf Se Te Zr In As
4 12 4 4 2 6
Direct
0.5094442192590720 0.5030120506135543 0.2901501052765245
0.0020690612295513 0.5009893591523656 0.2899526227434581
0.5096876852644945 0.0013750979789574 0.2901400173268417
0.0133989277795038 0.0066889173996939 0.2897358262041034
0.3411126970492526 0.1697825820659861 0.3395839434938758
0.3432691326482944 0.1704901923677284 0.1270028612740202
0.1763547525882629 0.3373188854388547 0.0246972728406681
0.8422005622400519 0.1705634786490660 0.3391833600142810
0.8431314092846749 0.1704096534976482 0.1270273347431942
0.6763685764141142 0.3372752932296402 0.0246640925601666
0.3441564692131688 0.6711027021915658 0.3395399865212277
0.3431497960856158 0.6704908934981822 0.1270669853920373
0.1764485105179100 0.8374105831227504 0.0247508197796830
0.8425213239555430 0.6682456856606621 0.3391392549537119
0.8431342163326622 0.6705567497117025 0.1270615159132901
0.6765065273713016 0.8374558790728105 0.0247419901336707
0.1762083198862491 0.3345129429229367 0.2295968614513502
0.6782135425474727 0.3388010731667437 0.2291007400247823
0.1757186273948257 0.8374606119694232 0.2297194313531283
0.6716903966846313 0.8357453583138573 0.2297592915864574
0.5097823505513300 0.5038179754548697 0.0757946393498289
0.0098419350939837 0.5038852241547526 0.0758191637716898
0.5097924051367456 0.0038730718560678 0.0758118927859355
0.0097443472880454 0.0038310487968546 0.0758455098266956
0.3259819184897683 0.6549650052469177 0.4530284431962250
0.6577234174826350 0.3225300538204609 0.4518035886337355
0.1397653014898118 0.8454698971708562 0.4339700144014551
0.7035392763813434 0.8464000967602542 0.4332548341228172
0.1373716641417300 0.2764502348347136 0.4348147760047984
0.2928121259082037 0.1381235185399631 0.4822239798082927
0.8416500678713132 0.6896961263136441 0.4802386956156554
0.8397938630898337 0.1395427104964870 0.4812399356165855

Supplemental INCAR1. The input parameters for the optimizations of geometrical structures.

```
SYSTEM=Trilayer
ISTART=0
PREC=Accurate
ALGO=Normal
GGA=PE
NSW=1000
EDIFFG=-0.01
IBRION=2
ISIF=3
NFREE=4
ENCUT=550
EDIFF=1E-06
LREAL= False
IVDW=13
NELM   = 500
POTIM=0.05
IDIPOL=3
LDIPOL=.TRUE.
ISMEAR=0
SIGMA=0.05
NCORE=8
NPAR=6
```

Supplemental INCAR1. The input parameters for the static calculations.

```
SYSTEM=Trilayer
ISTART =1
ICHARG = 0
GGA=PE
PREC = Accurate
#-------------
NCORE=8
NPAR=6
#--------
###----------------------HSE---------------------------------
ALGO=All
LHFCALC = .TRUE.
HFSCREEN = 0.2
TIME = 0.4
PRECFOCK  = Fast
# NKRED     = 2
#--------------------------------------------------------------------
```

```
#
NSW=0
IBRION=-1
ISIF=3
ENCUT=550
EDIFF = 1E-06
EDIFFG = -0.01
ISMEAR = 0
SIGMA = 0.05
NELMIN = 8
NELM=300
POTIM=0.01
IDIPOL=3
LDIPOL=.TRUE.
EMIN = -20
EMAX = 20
NEDOS=3001
LORBIT=11
LOPTICS= .TRUE.
LREAL = .FALSE.
LVTOT=.TRUE.
LVHAR=.TRUE.
LAECHG = .TRUE.
IVDW=13
```

References

1. N. Jena, A. Rawat, R. Ahammed, M. K. Mohanta, et, al. Emergence of high piezoelectricity along with robust electron mobility in Janus structures in semiconducting Group IVB dichalcogenide monolayers, *J. Mater. Chem. A.* 2018, **6**, 24885–24898.
2. L. Wan, D. Chen, W. Zeng, J. Li, S. Xiao. Hazardous gas adsorption of Janus HfSeTe monolayer adjusted by surface vacancy defect: A DFT study. *Surf. Interfaces*, 2022, **34**, 102316.
3. K. Terashima, I. Imai. Indirect absorption edge of ZrS_2 and HfS_2. *Solid. State. Commun*, 1987, **63**, 315.
4. Y. Tian, M. Zheng, Y. Cheng, Z. Yin, J. Jiang. Epitaxial growth of $ZrSe_2$ nanosheets on sapphire via chemical vapor deposition for optoelectronic application. *J. Mater.*

Chem. C, 2021, **9**,13954.

5. R. A. B. Villaos, H. N. Cruzado, J. S. C. Dizon, et, al. Evolution of the electronic properties of ZrX_2 (X= S, Se or Te) thin films under varying thickness. *J. Phys. Chem. C*. 2021, **125**, 1134–1142.
6. M. Abdulsalam, D. P. Joubert. Optical spectrum and excitons in bulk and monolayer MX_2 (M= Zr, Hf; X= S, Se). *Phys. Status. Solidi B*, 2016, **253**, 705–711.
7. S. Singh, Z. Zanolli, M. Amsler, B. Belhadji. Low-energy phases of Bi monolayer predicted by structure searching two dimensions. *J. Phys. Chem. Lett*. 2019, **10**, 7324−7332.
8. X. Zhang, X. Zhao, D. Wu, Y. Jing, Z. Zhou. $MnPSe_3$ monolayer: A promising 2D visible light photo hydrolytic catalyst with high carrier mobility. *Adv. Sci*, 2016, **3**, 1600062.
9. S. Saha, T. P. Sinha, A. Mookerjee. Electronic structure, chemical bonding, and optical properties of paraelectric $BaTiO_3$. *Phys. Rev. B*, 2000, **62**, 8828-8834.
10. P. Li, C. Zhang, J. Lian, M. Ren, P. Wang, X. Yu, et, al. First-principal study of optical properties of Cu-doped CdS. *Opt. Commun*, 2013, **295**, 45-52.
11. Y. Li, Z. Chen. Tuning electronic properties of germanane layers by external electric field and biaxial tensile strain: a computational study. *J. Phys. Chem. C*, 2014, **118**, 1148.
12. C. F. Fu, J. Sun, Q. Luo, X. Li, W. Hu, J. Yang. Intrinsic electric fields in two-dimensional materials boost the solar-to-hydrogen efficiency for photocatalytic water splitting. *Nano Lett*, 2018, **18**, 6312-6317.
13. C. Ling, L. Shi, Y. Ouyang, X. C. Zeng, J. Wang. Nanosheet supported single-metal atom bifunctional catalyst for overall water splitting. *Nano Lett*, 2017, **17**, 5133.
14. Q. Zheng, W. Chu, C. Zhao, L. Zhang, et al. *Ab initio* nonadiabatic molecular

dynamics investigations on the excited carriers in condensed matter systems. *Wiley Interdiscip. Rev.: Comput. Mol. Sci.* 2019, **9**, e1411.

15. R. Long, O. V. Prezhdo. Quantum coherence facilitates efficient charge separation at a MoS_2/$MoSe_2$ van der Waals junction. *Nano Lett*. 2016, **16**, 1996−2003.
16. H. M. Jaeger, S. Fischer, O. V. Prezhdo. Decoherence-induced surface hopping. *J. Chem. Phys*. 2012, **137**, 22A545.
17. J. P. Perdew, K. Burke, M. Ernzerhof. Generalized gradient approximation made simple. *Phys. Rev. Lett*. 1996, **77**, 3865.
18. S. Chen, L. W. Wang. Thermodynamic oxidation and reduction potentials of photocatalytic semiconductors in aqueous solution. *Chem. Mater*, 2012, **24**, 3659-3666.
19. Y. Xu, M. A. A. Schoonen. The absolute energy positions of conduction and valence bands of selected semiconducting minerals. *Am. Mineral*, 2000, **85**, 543-556.
20. X. Niu, D. Sun, L. Shi, X. Bai, Q. Li, X. Li, et al. A new nitrogen fixation strategy: the direct formation of $*N_2^-$ excited state on metal-free photocatalyst. *J. Mater. Chem. A.* 2021, **9**, 6214−6222.
21. G. Gao, A. P. O'Mullane, A. Du. 2D MXenes: a new family of promising catalysts for the hydrogen evolution reaction. *ACS Catal*, 2017, **7**, 494.
22. T. He, G. Gao, L. Kou, G. Will, A. Du. Endohedral metallofullerenes (M@C60) as efficient catalysts for highly active hydrogen evolution reaction. *J Catal*, 2017, **351**, 231.
23. D. Er, H. Ye, N. C. Frey, H. Kumar, J. Lou, V. B. Shenoy. Prediction of enhanced catalytic activity for hydrogen evolution reaction in Janus transition metal dichalcogenides. *Nano Lett*, 2018, **18**, 3943,18.